Materials Chemistry and Physics 226 (2019) 95–99

Contents lists available at ScienceDirect

Materials Chemistry and Physics

journal homepage: www.elsevier.com/locate/matchemphys

Large enhancement of the CDW resistivity anomaly and traces of superconductivity in imperfect samples of $NbTe_4$

B.S. de Lima[a,*], N. Chaia[a], T.W. Grant[a], L.R. de Faria[a], J.C. Canova[a], F.S. de Oliveira[a], F. Abud[b], A.J.S. Machado[a]

[a] Escola de Engenharia de Lorena, Universidade de São Paulo, Lorena, SP, 12600-970, Brazil
[b] Instituto de Física, Universidade de São Paulo, Rua do Matão 1371, 05508-090, São Paulo, São Paulo, Brazil

HIGHLIGHTS

- $NbTe_{4-\delta}$ samples were prepared through conventional solid state reaction within the range of $0 \leq \delta \leq 2$.
- Interstitial Te atoms enhances the resistivity anomaly related to the CDW transition.
- Te deficiency induces a superconductor state to emerge at 5.5 K.

ARTICLE INFO

Keywords:
$NbTe_4$
One-dimensional conductor
CDW
Superconductivity

ABSTRACT

Transition metal chalcogenides usually crystallize in low-dimensional structures that frequently host electronic instabilities such as charge density waves (CDW) and superconductivity. Among them is $NbTe_4$. This compound is a quasi-one-dimensional conductor that exhibits successive CDW transitions and superconductivity at 2.2 K when hydrostatic pressure is applied. The binary Nb-Te phase diagram predicts that this compound is non-stoichiometric and exists within a Te composition range. This work presents a systematic investigation of the physical properties of $NbTe_{4-\delta}$ polycrystalline samples. Electrical resistivity measurements show a large enhancement of the anomaly related to the CDW transition in the vicinity of 200 K. Further characterization demonstrates that Te deficiency can also induce superconductivity in this compound at 5.5 K and coexists with the CDW state.

1. Introduction

Transition metal chalcogenides (TMCs) compounds typically have formula such as MX_2, MX_3, and MX_4 where M is a transition metal and X = S, Se or Te. MX_2 compounds usually crystallize in layered-like structures that are frequently pointed out as examples of two-dimensional compounds [1]. On the other hand, MX_3 and MX_4 crystallize in quasi-one-dimensional structures [2,3]. Both families are well known as hosts of a great variety of electronic properties and instabilities, such as the formation of charge-density waves (CDW) and its competition with superconductivity as a ground state [4–7].

The idea that superconductivity and CDW are competitive states at low temperatures represents one of the fundamental concepts of condensed matter physics, because compounds that exhibit both phenomena may hold answers to a better comprehension of the mechanism of Cooper pair formation in high T_C superconductors [8]. In this scenario, several transition metal chalcogenides have been identified as compounds that exhibit both states under application of external pressure or chemical doping. It is worth citing some remarkable compounds such as 1T-$TiSe_2$ that undergoes a CDW transition close to 220 K and becomes superconductor below 4.15 K when Cu is intercalated between the Te-Te van der Waals bonds [4]. The same occur with TaS_2 under Na intercalation or under hydrostatic pressure [5,9]. $NbSe_2$ and $NbSe_3$ are well-known examples of coexistence of superconductivity and CDW under ambient conditions [10–13]. More recently, coexistence of CDW and superconductivity was observed in Hf and Zr based chalcogenides [14–16].

Within this context is $NbTe_4$. This compound crystallizes in a tetragonal structure, space group (SG) 124 (P4/mcc) that was first determined by Selte and Kjekshus in 1964 [17]. This structure can be pictured as a 3D parallel stacking of antiprism formed by the Te atoms in the apexes and a linear chain of Nb atoms in the center. Each Nb

* Corresponding author.
E-mail address: delima.bs@usp.br (B.S. de Lima).

https://doi.org/10.1016/j.matchemphys.2019.01.008
Received 31 May 2018; Received in revised form 14 December 2018; Accepted 4 January 2019
Available online 11 January 2019
0254-0584/

atom is surrounded by 8 Te atoms and this bonding structure leaves enough charge free for conduction in the d band of the Nb atoms. The low dimensional character of its structure hosts a propitious environment for CDW transitions.

It is well established that the structure determined by Selte and Kjekshus is, in fact, the average of an incommensurate modulated superstructure with wave vector of (½, ½, 0.688) [3]. This distortion happens in each Nb-Nb chain with a phase difference of π. The incommensurate structure undergoes a transition at 180 K that consists in an intermediate incommensurate state that some authors address as a discommensurate transition. In fact, the distortion vector of this superlattice changes its period of modulation in 16c'/2 [3]. At 50 K this discommensurate state undergoes a lock-in transition becoming a commensurate superstructure with wave vector of (2x2x3) [18]. All of these successive CDW transitions in $NbTe_4$ have been already observed by diffraction techniques, however, these transitions have a small effect on the electrical resistivity that was observed by S. Tadaki and collaborators. Tadaki et al. observed a small deviation of the linearity around 180 K in the derivative dρ/dT vs T [19]. At 50 K, the electrical resistivity data shows a small discontinuity that is related to the lock-in transition reported by D. J. Eaglesham et al. [18]. Recently, X. Yang et al. reported the CDW transition at 200 K, which is in agreement with our data [22]. It is important to mention that the effect of these CDW transitions on the electrical properties of the $NbTe_4$ is much smaller than the effects of the CDW transitions on the electrical resistivity of other compounds, such as $NbSe_3$ or 1T-TaS_2 [5,20]. Band structure calculations show that the conduction band consists of half-filled d_{z2} from the Nb atoms, and furthermore, three different CDW nesting vectors in the Fermi surface were identified that suggest three independent CDW states on this compound that depends on the position of the Nb-Nb chain [21]. Recently, a report demonstrated that external pressure can suppress the CDW state and simultaneously, a superconductor state emerges at 2.2 K [22].

This report aims to investigate the influence of Te content in the physical properties of $NbTe_4$. We present a systematic study on the preparation of polycrystalline samples with nominal composition of $NbTe_{4-\delta}$ in order to investigate the influence of Te deficiency (δ) in the crystal structure and in the physical properties of this quasi-one-dimensional conductor. Our results suggest that the presence of Te atoms in some interstitial positions can significantly increase the CDW anomaly in the electrical resistance around 200 K. Also, a superconductor state emerges at 5.5 K in the sample with the highest Te deficiency.

2. Experimental procedure

Polycrystalline samples of $NbTe_{4-\delta}$ with $0 \leq \delta \leq 2$ were prepared by powder metallurgy solid-state reaction. High purity powders of Nb (99.8%) and Te (99.998%) were weighted in the defined stoichiometric proportions, homogenized, pressed into pellets, sealed in a quartz tube under argon atmosphere, heat treated at 400 °C for 72 h and finally quenched in iced water. Then, the samples were grounded, homogenized, pressed into pellets and heat treated again at 400 °C for another 72 h and quenched in iced water. X-ray powder diffraction measurements were carried out at room temperature with 40 kV–30 mA, Cu-Kα radiation, and Ni filter. The 2θ data were collected from 10 to 90° using a step of 0.05°. X-ray diffraction data were analyzed using Rietveld refinement with the software PowderCell [23], Vesta Crystallography [24], and EXPGUI (GSAS) [25]. Magnetization, resistivity and heat capacity as a function of temperature measurements were carried out in a PPMS Evercool II from Quantum Designs. Magnetization was determined with zero field cooling (ZFC) and field cooling (FC) with an applied magnetic field of 20 Oe. Electrical resistivity as a function of temperature was measured using the standard four-probe method from 2 to 350 K.

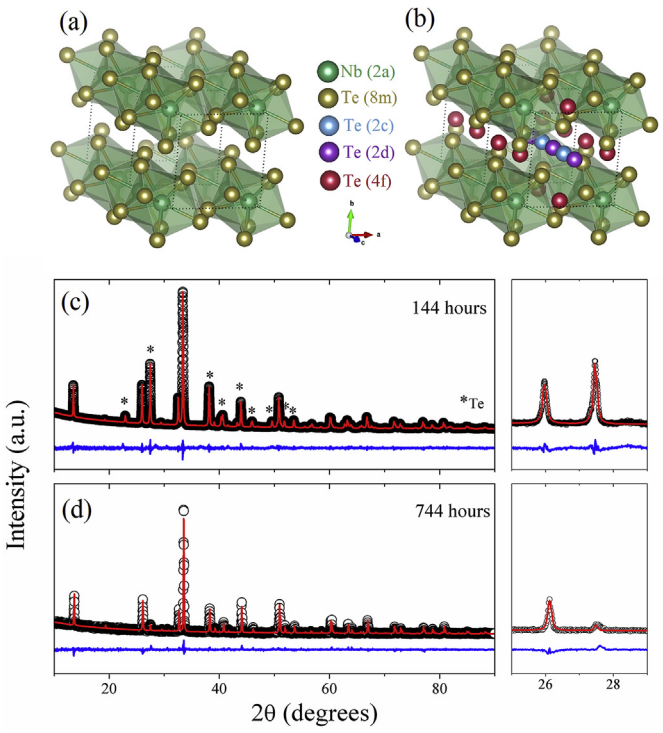

Fig. 1. Crystal structure of (a) NbTe4 and (b) NbTe4 with Te atoms occupying 2c, 2d, and 4f Wyckoff sites. (c) and (d) XRD data for samples heat treated at 400 °C over 144 and 744 h respectively. Right panels show the vicinity of regions in which pure Te peaks overlap with NbTe4 peaks.

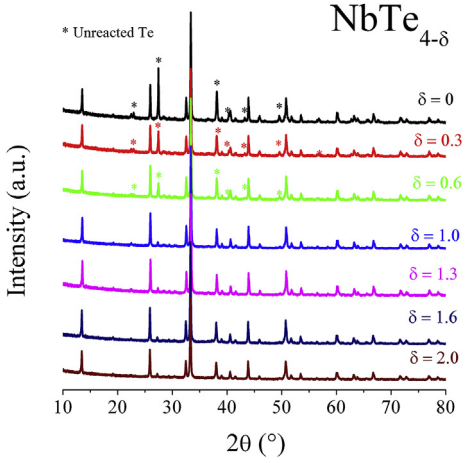

Fig. 2. X-ray diffraction pattern of NbTe4-δ samples with $2 \leq \delta \leq 4$.

3. Results and discussion

Before introducing the Rietveld Refinement results, our discussion will first illustrate some important features of the crystal structure and XRD patterns of these Te deficient samples. Fig. 1(a) presents the crystal structure of $NbTe_4$ proposed by Selte and Kjekshus [17]. It is possible to observe the Nb-Nb chain along the *c* axis gives $NbTe_4$ its quasi-one-dimensional character. Fig. 1(b) shows the same structure with Te atoms positioned in interstitial sites with Wyckoff positions of 2c, 2d, and 4f that are represented by blue, purple and red spheres respectively. The original structure proposed by Selte and Kjekshus [17] is tetragonal with SG P4/mcc, number 124, lattice parameters $a = b = 6.496$ Å and $c = 6.823$ Å. It is important to mention that pure tellurium crystallizes in hexagonal structure with SG $P3_121$, number 152, lattice parameters $a = b = 4.44$ Å and $c = 5.92$ Å. Hence, a powder X-ray

Table 1
Rietveld Refinement results of the XRD presented in Figs. 1 and 2.

Composition (δ)	NbTe4 (P4/mcc)			Te ($P3_121$)			χ^2	R_{WP}
	a (Å)	c (Å)	Weight Fraction	a (Å)	c (Å)	Weight fraction		
0.0[a]	6.5016	6.8359	1	–	–	0	1.347	10.08
0.0	6.4965	6.8232	0.801	4.4534	5.9211	0.199	1.924	7.96
0.3	6.5014	6.8329	0.896	4.4572	5.9258	0.123	1.798	7.80
0.6	6.5017	6.8326	0.918	4.4563	5.9257	0.082	1.911	7.88
1.0	6.5025	6.8338	1	–	–	0	2.073	8.24
1.3	6.5036	6.8344	1	–	–	0	1.767	7.77
1.6	6.5025	6.8338	1	–	–	0	2.136	8.23
2.0	6.5025	6.8338	1	–	–	0	1.936	7.93

[a] Rietveld refinement data from the XRD shown in Fig. 1(d).

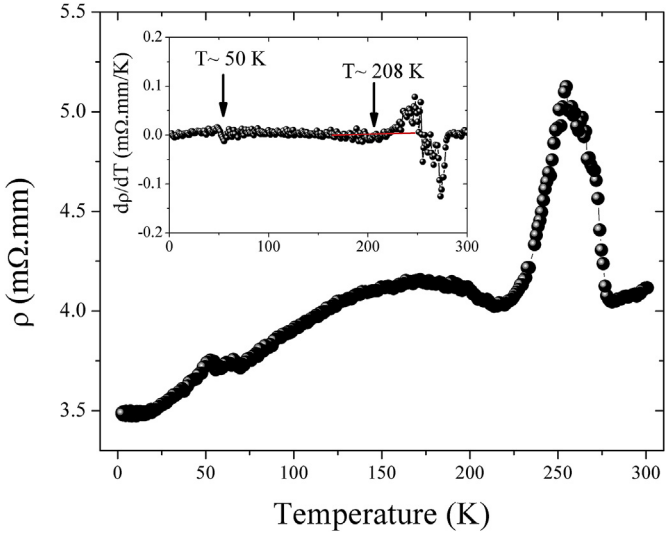

Fig. 3. Electrical resistivity as a function of temperature for a sample prepared with nominal composition of $NbTe_4$. Nonlinear behavior shows two transitions related to the formation of the CDW transitions [3,18,19].

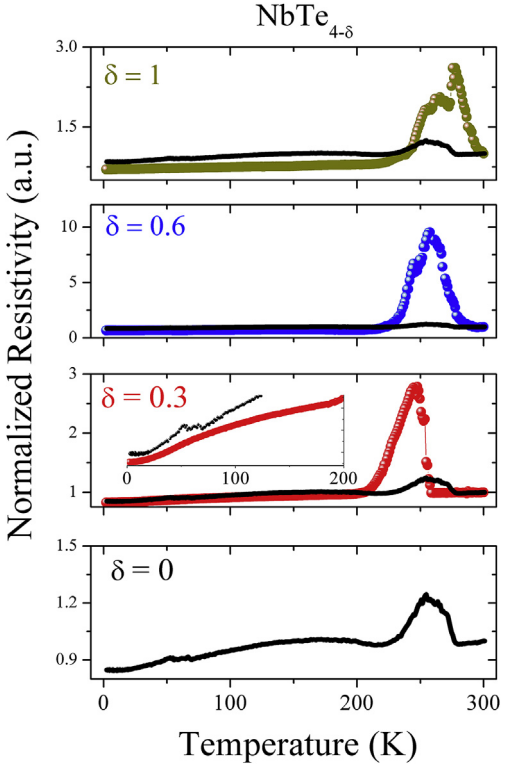

Fig. 4. Normalized resistivity for $NbTe_{4-\delta}$ samples. From lower to upper panel, δ = 0, 0.3, 0.6 and 1 respectively. For comparison, the curve for δ = 0 is plotted with the other curves in black. The Inset shows the low-temperature resistivity data of the samples δ = 0 and δ = 0.3.

diffraction pattern of a real mixture of these two phases would exhibit an overlap of several peaks. This is the case of peaks close to 2θ = 27.3, 38.1, 40.6, 46 and 51.8° and etc. Fig. S1 in the Supplementary Material shows a simulation of the XRD data of these two phases plotted together where it is possible to observe the proximity of some diffractions peaks. Fig. 1(c) and (d) presents X-ray diffraction data and the Rietveld Refinement of two samples with nominal composition of $NbTe_4$ prepared at 400 °C over 144 h of heat treatment (Fig. 1(c) and a sample prepared at 400 °C over 744 h (Fig. 1(d)). The right panels illustrate the region in the vicinity of 27°.

One can observe in Fig. 1 (c) and (d) that the sample prepared with 144 h of heat treatment have much more intense peaks related with unreacted Te in comparison with the sample treated during 744 h. In fact, the presence of Te in samples prepared with nominal composition of $NbTe_4$ at 400 °C is expected [26]. According to the peritectic transformation predicted in the Nb-Te phase equilibria diagram (Te (l) + $NbTe_3$(s) = $NbTe_4$) the optimal composition should be at 79 at. % of Te instead of 80 at. % [26]. For the sample treated over 144 h, the lattice parameters obtained with the Rietveld Refinement were $a = b = 6.503$ Å, $c = 6.835$ Å for the $NbTe_4$ (SG P4/mcc) phase and $a = 4.458$ Å $c = 5.927$ Å for the Te phase (SG $P3_121$). Furthermore, the Rietveld Refinement allowed us to estimate the amount of Te present in which of the Wyckoff sites pointed out in Fig. 1(b). In the sample treated over 744 h, the Refinement converged fast and yielded error parameters of $\chi^2 = 1.447$, $R_{WP} = 10.45\%$ with Nb and Te occupancy factor of 1 at the 2a and 8m Wyckoff positions respectively. This result suggest that 744 h of heat treatment is enough time to Te atoms sit in the predicted position proposed by Selte and Kjekshus [17]. On the other hand, the sample treated over 144 h showed occupancy factors of 0.8559 and 0.8941 for the Nb 2a and Te 8m. Also, the Refinement showed that some of the 2c and 2d positions are occupied by Te atoms, with occupancy factors of 0.1357 and 0.0869. This Refinement had errors parameters estimated in $\chi^2 = 1.94$ and $R_{WP} = 7.96\%$. The Te weight fraction was estimated at 0.199. It is important to mention that if one does not consider Te in the refinement, the smallest errors parameters obtained for this sample are $\chi^2 = 9.862$, $R_{WP} = 18.03\%$. These results demonstrate that after 144 h of heat treatment the solid-state reaction was not complete, with some Te atoms occupying intermediate positions between the main antiprisms chain and with some unreacted Te present in the sample. All the structural parameters of the Rietveld Refinement of these samples are shown in Tables S1 and S2 in the Supplementary Material.

Fig. 2 presents X-ray diffraction data for samples prepared with nominal composition of $NbTe_{4-\delta}$ ($0 \leq \delta \leq 2$) heat treated over 144 h in 400 °C. Table 1 summarizes the results of the Rietveld refinement of

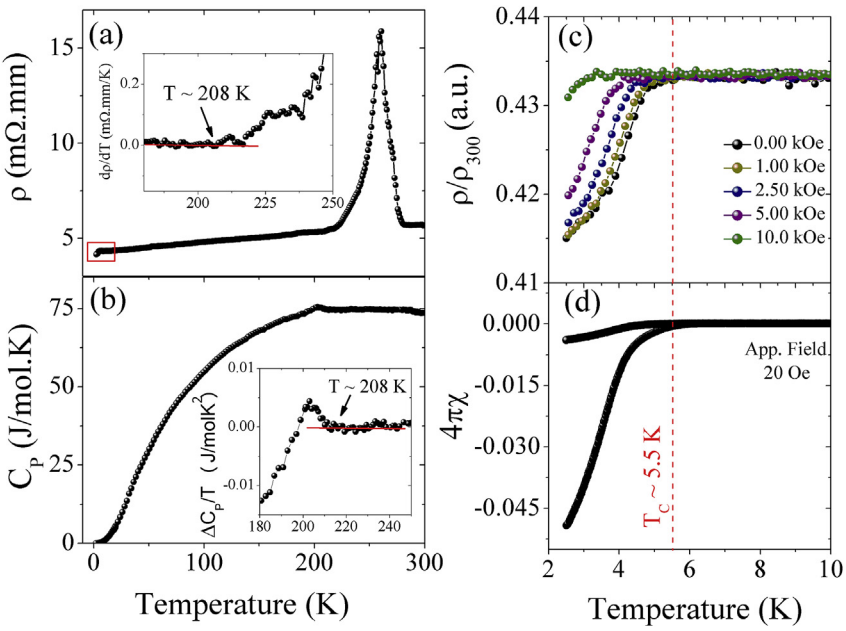

Fig. 5. Experimental data for a sample with nominal composition of δ = 2. (a) Electrical resistivity as a function of temperature. The inset presents the derivative as a function of temperature to define the transition temperature in T_{CDW} ~208 K. (b) Specific heat as a function of temperature. The inset shows $\delta C_P/T$ as a function of temperature. A small discontinuity is observed in the vicinity of 208 K. (c) Low-temperature resistivity data with different applied magnetic fields. (d) ZFC and FC magnetic susceptibility for 20 Oe showing a superconducting transition at 5.5 K.

these samples. One can observe in Fig. 2 that the relative intensities of the peaks related with unreacted Te decrease monotonically with the Te deficiency (δ). This is also confirmed by the amount of unreacted Te fraction in Table 1. In samples with δ ≥ 1 (nominal composition of $NbTe_3$) the Rietveld analysis does not show any other phases rather than $NbTe_4$ which can be seen in further details in Table 1. Another feature of these samples is that the Te content has no effect upon the lattice parameter of the $NbTe_4$ phase as one can notice in the calculated lattice parameters shown in Table 1.

Another important feature of these samples is related to the occupancy factor of the Nb (2a) and Te (8m). One can observe that Te defects in the 8m positions are accompanied by Nb defects in the 2a positions to maintain the neutrality of the system. It is possible to observe that all of these samples have Te atoms located in the 2c and 2d Wyckoff positions. However, only samples with δ = 0.3 and 0.6 have some Te atoms in the 4f positions with an occupancy factor of 0.0009 and 0.0198 respectively. Figs. S2 and S3 present the average atoms per unit cell for each of the samples. The average number of Te atoms per unit cell is 7.96, which is the maximum value for the sample with deficiency of δ = 0.6. This estimation can be carried out by multiplying the occupancy factor and the multiplicity of each Wyckoff position. The ratio of Te/Nb atoms is approximately the same for all the samples and was estimated in 4.4 ± 0.1. From Figs. S2 and S3, it is possible to observe that the sample with δ = 0.6 has the highest value Te atoms per unit cell, while the sample with δ = 2 has the lowest.

Now, let us turn the discussion to the electrical properties of these Te deficient samples. Fig. 3 exhibit the electrical resistivity data as a function of temperature for the sample with nominal composition of $NbTe_4$ treated over 144 h. In Fig. 3 one can observe two clear transitions that had its temperature defined after the deviation from linearity in the dρ/dT curve (inset). By this criterion, one can estimate the transitions temperatures as 208 K and 50 K. In fact, these values are in agreement with the temperature for the CDW transitions that have been reported for single-crystalline samples of $NbTe_4$. Diffraction studies show that the incommensurate transition happens in the vicinity of 180 K [3]. Even though X-ray diffraction data demonstrated that this sample exhibit unreacted Te, we argue that the electrical behavior observed in the data presented in Fig. 3 is related to the $NbTe_4$ phase. Our argument is based on the fact that Te has electrical resistivity of 0.5 and 10 Ω.cm at room temperature and at 2 K respectively [27], which are values four orders of magnitude larger than what is observed in the sample of the present work. Hence, the electronic path would take place in the lowest resistivity phase, which is $NbTe_4$. The other Te deficient samples were also characterized by the four probe method, in order to better understand the influence of Te deficiency in the electrical properties of the $NbTe_4$. Fig. 4 presents electrical resistivity as a function of temperature for the samples in which δ = 0, 0.3, 0.6, and 1.

The results presented in Fig. 4 demonstrate that the anomaly related to the intermediate incommensurate transition at 208 K increases dramatically by increasing the Te deficiency. For comparison, the curve related to the sample of nominal composition $NbTe_4$ were plotted together with all the other samples (black curve). When δ = 0.3, the maximum in the normalized resistivity curve (ρ/ρ_{300}) reaches 3 and surpasses 10 when δ = 0.6. It is important to emphasize that these samples are the only samples that exhibit Te atoms occupying the 4f Wyckoff positions. This value decreases again to 3 when δ = 1 and seems to stabilize in other samples with higher Te deficiency contents. It is important to point out that samples with Te deficiency of δ ≥ 1 are single-phased according to the XRD data presented in Fig. 2 and Table 1. The inset in the δ = 0.3 (red dots in Fig. 4) shows that the low-temperature anomaly is suppressed as it was not observed in samples with higher Te deficiency. Another sample with nominal composition of $NbTe_2$ (δ = 2) had its electrical properties also evaluated. These results are presented in Fig. 5.

The CDW anomaly at 208 K is also present in the sample prepared with nominal composition of $NbTe_2$, as it can be seen in Fig. 5(a). The inset shows the deviation from linearity in the derivative curve as a criterion to define the transition temperature. Surprisingly, however, this sample also exhibits the emergence of a superconducting state at *Tc* ~5.5 K. Regarding Te atoms positioning, it is important to mention that this sample is the only one that exhibit 2d Wyckoff empty vacant and still several positions of Nb (2a) and Te(8m) unoccupied. The resistivity drop due to this transition is pointed out in the red square and can be seen in further details in Fig. 5(c). Specific heat as a function of temperature is presented in Fig. 5(b). One can observe a small jump in the vicinity of 208 K which is in agreement with the resistivity data. Fig. 5(c) shows the electrical resistivity in the low temperature region. The superconducting transition is clear and the T_C shifts towards low temperature as magnetic field increases. Magnetization data is presented in Fig. 5(d). The superconducting volume was estimated with the magnetization data in 4.5%. The small superconducting fraction explains why the resistance does not drop to zero and why it is not

possible to observe the superconducting characteristic jump in its heat capacity curve. The small superconducting fraction can be explained due to chemical inhomogeneity of Te.

4. Conclusions

This report demonstrated an experimental procedure to synthesize Te deficient polycrystalline samples of NbTe4. It is shown that Te deficient samples exhibit Te atoms occupying interstitial positions of the original crystal structure of NbTe4. This defective structure causes a large enhancement of the electrical resistivity anomaly related with a CDW ordering around 200 K. It is shown that this enhancement achieves a maximum point in a sample with deficiency $\delta = 0.6$. It is shown that further increase of Te deficiency does not affect the CDW state and causes a superconducting state to emerge in samples when $\delta = 2$. The superconducting transition temperature is equal to 5.5 K. This works opens a research perspective to study Te deficient NbTe4 single crystals, and the dynamics of Te positioning by neutron diffraction techniques. Also, to study whether hydrostatic pressure is able to suppress the CDW transition and enhance the superconducting fraction observed in these samples.

Acknowledgements

This work is based upon financial support by the Brazilian research agencies CAPES, CNPq (302850/2014-7, 443385/2014-9 and 142016/2013-6) and FAPESP (2013/16873-3 and 2016/11774-5).

Appendix A. Supplementary data

Supplementary data to this article can be found online at https://doi.org/10.1016/j.matchemphys.2019.01.008.

References

[1] J.A. Wilson, F.J. Di Salvo, S. Mahajan, Adv. Phys. 50 (2001) 1171.
[2] Z.X. Dai, C.G. Slough, R.V. Coleman, Phys. Rev. Lett. 66 (1991) 1318.
[3] F.W. Boswell, A. Prodan, J.K. Brandon, J. Phys. C Solid State Phys. 16 (1983) 1067.
[4] E. Morosan, H.W. Zandbergen, B.S. Dennis, J.W.G. Bos, Y. Onose, T. Klimczuk, A.P. Ramirez, N.P. Ong, R.J. Cava, Nat. Phys. 2 (2006) 544.
[5] B. Sipos, A.F. Kusmartseva, A. Akrap, H. Berger, L. Forro, E. Tutis, Nat. Mater. 7 (2008) 960.
[6] A.H. Castro Neto, Phys. Rev. Lett. 86 (2001) 4382.
[7] Q.H. Wang, K. Kalantar-Zadeh, A. Kis, J.N. Coleman, M.S. Strano, Nat. Nanotechnol. 7 (2012) 699.
[8] J. Chang, et al., Nat. Phys. 8 (2012) 871.
[9] L. Fang, Y. Wang, P.Y. Zou, L. Tang, Z. Xu, H. Chen, C. Dong, L. Shan, H.H. Wen, Phys. Rev. B 72 (2005) 014534.
[10] P. Garoche, J.J. Veyssie, P. Manuel, P. Molinie, Solid State Commun. 19 (1976) 455.
[11] H. Wang, et al., Nat. Commun. 8 (2017) 394.
[12] A. Briggs, P. Monceau, M. Nunezregueiro, J. Peyrard, M. Ribault, J. Richard, J. Phys. C Solid State Phys. 13 (1980) 2117.
[13] M. Ido, Y. Okayama, T. Ijiri, Y. Okajima, J. Phys. Soc. Jpn. 59 (1990) 1341.
[14] S.J. Denholme, A. Yukawa, K. Tsumura, M. Nagao, R. Tamura, S. Watauchi, I. Tanaka, H. Takayanagi, N. Miyakawa, Sci. Rep. 7 (2017) 45217.
[15] Y.P. Qi, et al., Phys. Rev. B 94 (2016) 054517.
[16] Y.W. Hu, F.P. Zheng, X. Ren, J. Feng, Y. Li, Phys. Rev. B 91 (2015) 144502.
[17] K. Selte, A. Kjekshus, Acta Chem. Scand. 18 (1964) 690.
[18] D.J. Eaglesham, D. Bird, R.L. Withers, J.W. Steeds, J. Phys. C Solid State Phys. 18 (1985) 1.
[19] S. Tadaki, N. Hino, T. Sambongi, K. Nomura, F. Levy, Synth. Met. 38 (1990) 227.
[20] J. Chaussy, P. Haen, J.C. Lasjaunias, P. Monceau, G. Waysand, A. Waintal, A. Meerschaut, P. Molinie, J. Rouxel, Solid State Commun. 20 (1976) 759.
[21] M.H. Whangbo, P. Gressier, Inorg. Chem. 23 (1984) 1228.
[22] X.J. Yang, et al., Sci. Rep. 8 (2018) 6298.
[23] G. Nolze, W. Kraus, Powder Diffr. 13 (1998) 256.
[24] K. Momma, F. Izumi, J. Appl. Crystallogr. 44 (2011) 1272.
[25] B.H. Toby, J. Appl. Crystallogr. 34 (2001) 210.
[26] D.L. Smith, A.R. Mochel, J.A. Maguire, J.J. Banewicz, J. Less Common. Met. 26 (1972) 139.
[27] G. Fischer, G.K. White, S.B. Woods, Phys. Rev. 106 (1957) 480.